International Journal of Research
Available at https://edupediapublications.org/journals
Special Issue on Conference Papers
e-ISSN: 2348-6848
p-ISSN: 2348-795X
Volume 05 Issue 06
March 2018

Effect of Friction Stir Welding Parameters (Rotation and Transverse) Speed on the Transient Temperature Distribution In Friction Stir Welding Of Aa 7020-T53

N. HARIKRISHNA
HOD, Dept of mechanical, Vidya Bharathi Institute of Technology, pembarthi (v)
Jangaon

ABSTRACT
Three-dimensional nonlinear thermal numerical simulations are conducted for the friction stir welding (FSW) of AA 7020-T53. Three welding cases with tool (rotational and travel) speeds of 900rpm-40mm/min, 1400rpm-16mm/min and 1400rpm-40mm/in are analyzed. The objective is to study the variation of transient temperature in a friction stir welded plate of 5mm workpiece thickness. Based on the experimental records of transient temperature at several specific locations during the friction stir welding process for the AA 7020-T53, thermal numerical simulation is developed. The numerical results show that the temperature field in the FSW process is symmetrically distributed with respect to the welding line, increasing travel speed decreasing transient temperature distribution and increasing rotational speed increase temperature distribution. Experimental data illustrates that peak temperatures are higher on the advancing side than the retreating side. Comparison with the temperature measured by the thermocouples records shows that the results from the present numerical simulation have good agreement with the test data.
Keywords: friction stir welding, transient temperature, temperature distribution, simulation.

INTRODUCTION

Friction stir welding (FSW) is a significant manufacturing process for producing welded structures in solid state [1]. This process offers several advantages compared to the conventional welding methods including higher mechanical properties and lower residual stresses as well as reduced occurrence of defects [2]. In FSW process, a rotating tool having a shoulder moves along the welding line. Rotational motion of the shoulder generates frictional heat leading to a softened region around the pin while the shoulder prevents deforming material from being expelled. In fact, a weld joint is produced by the extrusion of material from the leading side to the trailing side of the tool [3]. Flow pattern and temperature variations during the process are important to engineers for an appropriate designing of welding layout. Both experimental procedures and mathematical models have been utilized to understand material behavior during FSW process. For instance, Tang *et al*., [4] have measured thermal profile in FSW. They showed that temperature distribution was symmetric around the weld centerline, and the peak temperature at the weld center of Al 6061-T6 specimen was predicted about 450°C. Chao *et al*., [5] have experimentally studied heat transfer during FSW. They concluded that about 95% of heat generated from the friction was transferred into the workpiece, and the rest flowed into the tool as well as about 80% of the plastic work was dissipated as heat of deformation. Cao and Kou [6] have studied microstructural phenomena in FSW of AA 2219. Dickerson and Przydatek [7] have investigated formation of defects in FSW butt joints under different welding conditions. Guerra *et al*., [8], Li *et al*., [9], and Colligan [10] have investigated the material flow during FSW. Sutton *et al*., [11] have studied microstructural aspects during FSW of AA 2024.

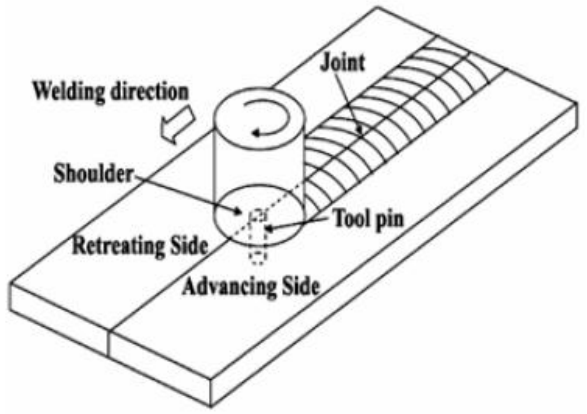

Figure-1. Schematic diagram shows friction stir welding

process and terminology. Several works on modeling of heat transfer and material flow during FSW have also been performed. Askari *et al*., [12] have used a 3D finite difference hydrodynamics code to establish the coupling between tool geometry, heat generation, and plastic flow during FSW process. Zhao [13] has simulated the material flow around the tool using LS-DYNA code. In this study, arbitrary Lagrangian- Eulerian formulations have been used with a "moving mesh" in order to handle severe plastic deformation around the rotating tool. Colegrove and Shercliff [14] have proposed a 2D model for determining material flow around the welding tool using commercial code based on fluid dynamic formulations, Fluent. Another study has been conducted by Hyoe *et al*., [15]. They investigated hardness profile across a weld and thermal histories as a function of position in the weld cross-section. The thermal history in their works was simulated by applying a uniform heat flux over the contact surfaces and a prescribed power input. Schmidt and Hattel [16] have used a commercial FE code, ABAQUS, to predict severe plastic deformation during FSW process. Nandan *et al*., [17] have presented a 3D visco-plastic finite element model for solving a coupled thermomechanical problem during FSW operations. Ulysse [18] has also used a visco-plastic approach to model 3D heat transfer and plastic flow during FSW where it has been assumed that heat is mainly generated from the rotational motion of the shoulder. Song and Kovacevic [19] have established a moving coordinate system to make easier modeling of FSW process. In their model, heat input has been generated from the tool shoulder and the tool pin. Chao and Qi [20] have assumed a constant heat flux input from a tool shoulder-sample interface. They have used a 3D heat transfer model using a trial and error procedure in order to adjust the heat input until all calculated temperatures matches with the measured values. Xu *et al*., [21] have developed a numerical model to predict the main thermomechanical features occurring in the FSW process. Objective of this study was to predict numerical thermal distribution in Al7020-T53. Plates that were welded by friction stir welding method in which effect of tool (advancing) travel speed and rotation speed were studied. For validation of numerical predictions, numerical findings were compared with experimental data measured by using thermocouples at location in mid position along welding tool path.

EXPERIMENTAL PROCEDURES

Friction stir welds were made on the plate samples of 7020-T53 aluminum alloy, with 5-mm thickness was cut out of the raw material. Single-pass friction stir butt welds were made using an FSW tool was fabricated from a tool steel labeled as X12M, The tool had a concaved shoulder (2o), while the tool pin is made cylindrical with a right hand threads of (1mm) pitch and have a round bottom. The overall height of the pin is (4.7mm), making slightly shorter than the plate thickness with shoulder diameter (18mm) and pin diameter (6mm) as shown in Figure-2. The welded plate are AA 7020-T53 Al alloy, each is in rectangular shape with a size of (153*95*5 mm). The tool is considered a rigid solid, and the work piece is considered a ductile material characterized with elasticity, plasticity and kinetic hardening effect. The temperature-dependent properties of 7020-T53 Al alloy at various temperatures are plotted in Figure-3 [22]. The employed welding parameters are (1400rpm-40mm/min), (1400rpm-16mm/min) and (900rpm-40mm/min). K-type thermocouples of 1.5 mm diameter were employed for

measuring the temperature variations at different positions of some samples. Figure-4 shows the positions of thermocouples. Thermocouples were attached Transient temperatures are recorded in the 12channels during FSW process; thermocouples are attached to SD card data logger temperature recorder (BTM-4208SD) as shown in Figure-5. Experimental works are conducted under different welding rotational speed in order to use the measured vertical loads and temperature results for verification of the accuracy of the modeled ones. Four cases are considered with differing tool rotational speeds (710rpm, 900rpm, 1120rpm and 1400rpm) a component dynamometer based on load cell (SEWHA, 2000kg capacity, R.O:2.0008mV/V) is used for measuring the vertical force during the FSW process for penetration time 60sec after that tool is moving with constant travel speed.

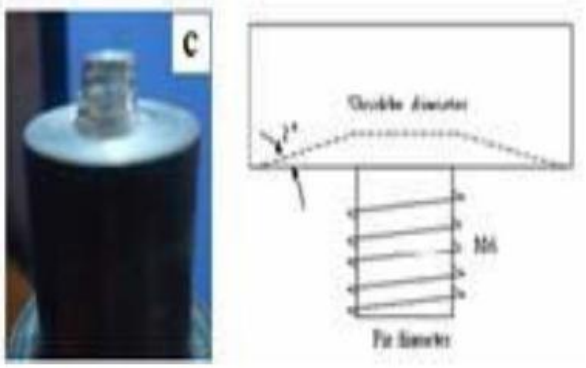

Figure-2. The configuration of the tool used.

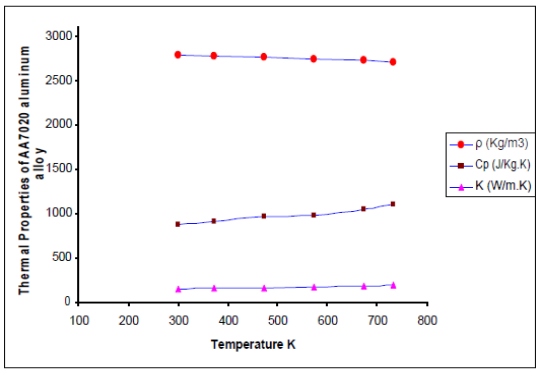

Figure-3. Thermal material properties of AA 7020-T53 Al alloy [22].

Figure-4. Temperature recorder and hole drill thermocouple position on workpiece.

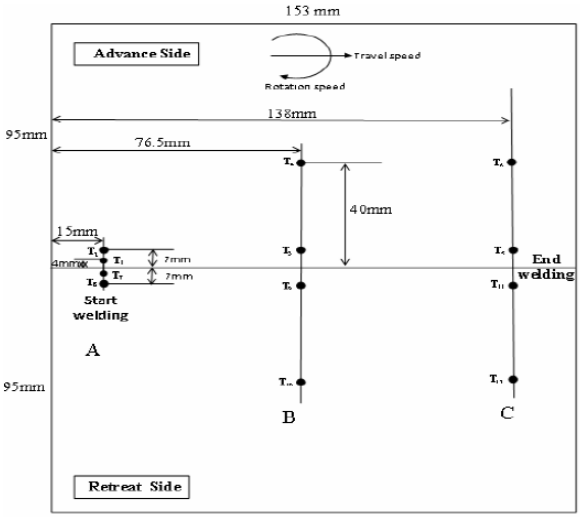

Figure-5. Thermocouple positions on the workpiece.

Finite element model

The thermal and mechanical responses of the material during friction stir welding process are investigated by finite element simulations. In this study, a nonlinear, transient three-dimensional heat transfer model is developed to determine the temperature fields The finite element models are parametrically built using APDL (ANSYS Parametric Design Language) provided by ANSYS® [23]. The models are then validated by comparing the results with experimental thermocouples data.

Thermal model

The purpose of the thermal model is to calculate the transient temperature fields developed in the workpiece during friction stir welding. In the thermal analysis, the transient temperature field T which is a function of time t and the spatial coordinates

(*x*, *y*, *z*), is estimated by the three dimensional nonlinear heat transfer equation (1).

$$k\left(\frac{\partial^2 T}{\partial^2 X}+\frac{\partial^2 T}{\partial^2 y}+\frac{\partial^2 T}{\partial^2 X}\right)+Q_{int}=c\rho\frac{\partial T}{\partial t} \quad (1)$$

Where *k* is the coefficient of thermal conductivity, *Qint* is the internal heat source rate, *c* is the mass-specific heat capacity, and ρ is the density of the materials. The heat transfer model developed for the thermal analysis is described in the following section.

Assumptions

A number of assumptions have been made in developing the finite element thermal model, which includes:

- Workpiece material is isotropic and homogeneous.
- No melting occurs during the welding process.
- Thermal boundary conditions are symmetrical across the weld centerline.
- Heat transfer from the workpiece to the clamp is negligible.

Elements used

In the present thermal analysis, the workpiece is meshed using a brick element called SOLID70. The element is defined by eight nodes with temperature as single degree of freedom at each node and by the orthotropic material properties.

Boundary condition

Boundary condition for FSW thermal model were specified as surface loads through ANSYS® codes. Assumptions were made for various boundary conditions based on data collected from various published research papers [24, 25]. Convective and radiative heat losses to the ambient occurs across all free surfaces of the workpiece and conduction losses occur from the workpiece bottom surface to the backing plate. To consider convection and radiation on all workpiece surfaces except for the bottom, the heat loss *qs* is calculated by equation (2).

$$q_s=\beta\,(T-T_o)+\varepsilon\,F\sigma(T^4-T_o^4) \quad (2)$$

where *T* is absolute temperature of the workpiece, *To* is the ambient temperature, *β* is the convection coefficient, is the emissivity of the plate surfaces, and σ = 5.67×10-8 W/m2 °K4is the Stefan-Boltzmann constant.

In the current model, a typical value of *β* was taken to be 30 *W*/*m*2K at ambient temperature of 300 K and was taken to be (0.5) for aluminum alloy F is radiation view factors (F=1). In order to account for the conductive heat loss through the bottom surface of weld plates, a high overall heat transfer coefficient has been assumed. This assumption is based on the previous studies [26]. The heat loss was modeled approximately by using heat flux loss by convection given by equation (3).

$$q_b=\beta_b\,(T-T_o) \quad (3)$$

where is a fictitious convection coefficient. Due to the complexity involved in estimating the contact condition between the welded plate and the backing plate, the value of had to be estimated by assuming different values through reverse analysis approach. In this study, the optimized value of was found to be (100-300) *W*/*cm*2oC. Figure-6 shows the schematic representation of boundary conditions that were used for thermal analysis.

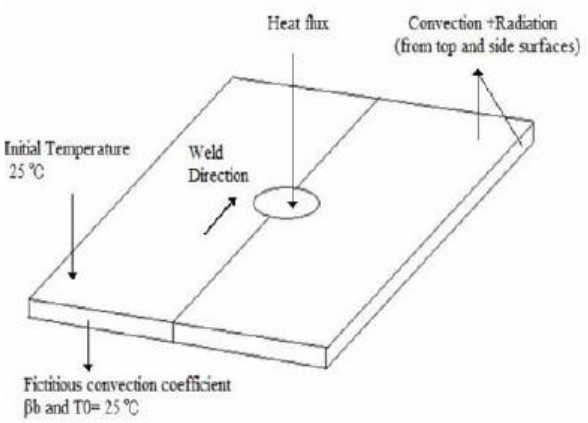

Figure-6. Schematic representation of boundary condition for thermal analysis.

Heat generation during friction-stir welding arises from two main sources: deformation of the material around the tool pin and the friction at the surface of the tool shoulder. A major difficulty is determining suitable values for the friction coefficient. The conditions under the tool are both extreme and very difficult to measure. To date, these parameters have been used as 'fitting parameters' where the model works back from measured thermal data to obtain a reasonable simulated thermal field. While this approach

is useful for creating process models to predict, for example, residual stresses it is less useful for providing insights into the process itself. Mathematical approximations for the total heat generated by the tool shoulder may be used to compensate for deformation heat generation; this could be done by an adjusting coefficient of friction. Friction is a complex physical phenomenon that depends on parameters like material, surface roughness, lubrication, temperature and pressure. The effects of friction in metal forming simulations are commonly accounted for by Coulomb friction models [26]. Assuming slipping conditions, the friction coefficient is adjusted in order to calibrate the model. A wide range of published values for friction coefficient is within 0.3-0.85 [27], which reflect the experimental conditions.

Total frictional heat of shoulder at rubbing angular speed $(1-\delta)\omega$, will be:

$$Q_s = \frac{2}{3}\pi(1-\delta)\omega\mu P R_s \quad (4)$$

where is the slip factor that compensate for tool/material relative velocity. Typical values for slip factor found in literature ranges between 0.6, 0.85 [28]. In similar concept, heat generated by lateral surface of the pin is:

$$Q_p = 2\pi(1-\delta)\,\omega\,\mu\,P L_p\,R_p^2 \quad (5)$$

Total frictional heat generated by the tool is the summation of equations (4) and (5) which is:

$$Q_T = 2\pi(1-\delta)\omega\mu P\left(\frac{R_s^3}{3} + L_p\,R_p^2\right) \quad (6)$$

Simulation

The thermal modeling was carried out in transient thermal analysis Figure-5 illustrates the flow diagram of the method used for the finite element analysis. Since the problem involves nonlinear analysis, full Newton-Raphson option was used to solve the nonlinear equations.

RESULTS AND DISCUSSIONS

During the penetration phase, the rotating tool pin penetrates into the workpiece until the tool shoulder comes contact with the workpiece. The penetration speed is chosen to be (0.0783mm/sec) in the model, and the corresponding penetration time is approximately (80sec). convection heat transfer coefficient with backing plate (300W/m2k), convection heat transfer coefficient (30W/m2k), ambient and initial temperature (To = 293K), slip factor (δ = 0.6), friction coefficient (μ = 0.41), (axial load = 2kN), Heat generation(Q = 331watt) used as input welding parameters in the finite element calculation with their corresponding vertical force in the workpiece predicted in Figure-7 the plasticization of material under the tool increase with increase rotational speed and with decrease in tool traverse speed resulting the reduction of vertical force. The finite element simulation couples the moving tool with the workpiece and also considers the thermal effect of the initial tool pin penetration before start of the weld.

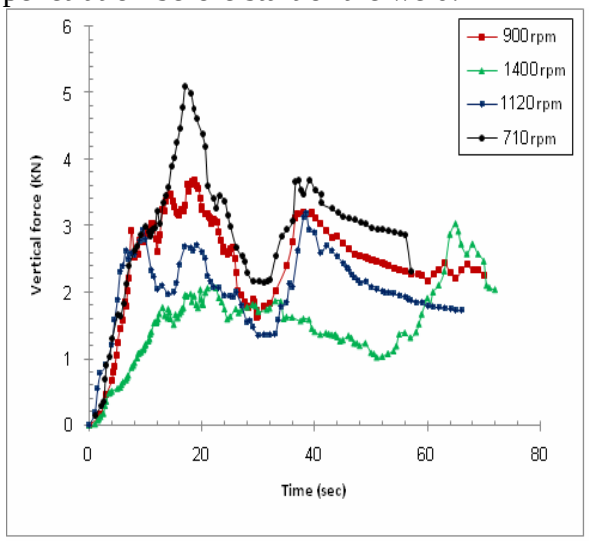

Figure-7. Vertical force penetration of tool on the workpiece during the FSW process.

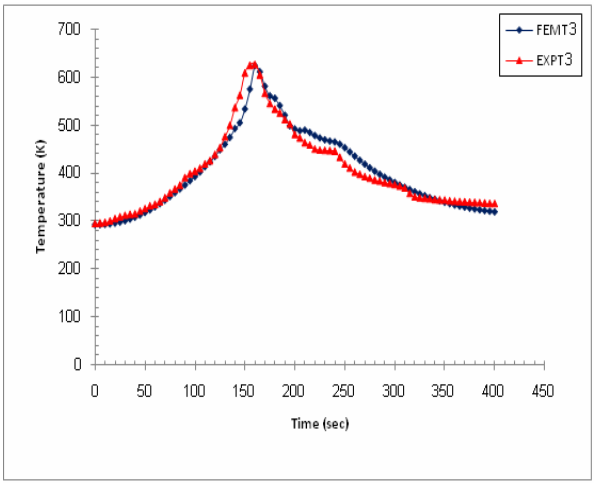

Figure-8. Comparison of the modeled and measured temperature history for thermocouple T3 location 7mm from joint line on advance side in section B-B.

Figure-8 shows comparison of experimental value and F.E modeled value for thermocouple T3 in section B-B while the tool traveled at mid position along tool movement in welding line at time 160sec.

Figure-9 shows that peak temperature resulting from transient thermal modeling analysis is more than experimental results because of the lake of accuracy in modeling of heat transfer. In actual case heat transfer through the fixture will increase the cooling process of the workpiece. The results obtained from transient thermal modeling were more accurate for workpiece of small dimensions relative to the heat source. Section B-B located at middle position at y = 76.5mm, four thermocouples two (T3 and T4) in advance side and two (T9 and T10) in retreate side, T3 and T9 located in 7mm in transverse of welding line (under shoulder surface when tool pass over this area).

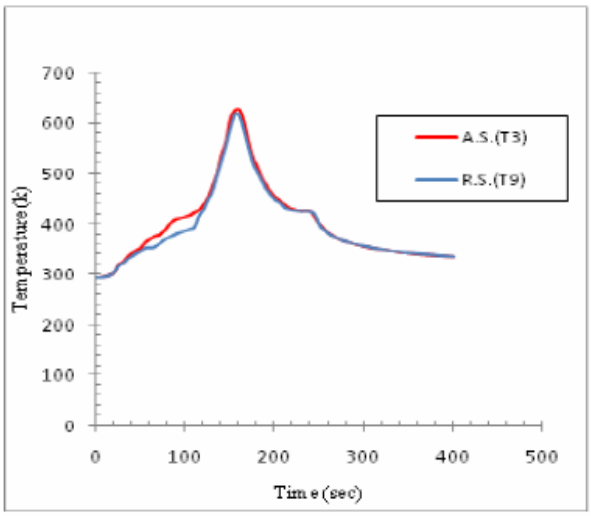

Figure-9. Comparison thermocouples measured value in advance T3 and retreate side T9 at section B-B (ω = 1400rpm and VT = 40 mm/min).

Experimental result shows that the temperature in advance side is higher than retreate side because material flow and plastic deformation around tool is moving from advance side to retreate side additional to friction heat under the shoulder that gives higher temperature. The computational results show that the material flows on the retreating and the front sides are higher. So, the slipping rates on the retreating and the front sides are lower than the ones on the trailing and advancing sides. This is the reason that the heat fluxes on the trailing and the advancing sides are higher, which leads to the fact that the temperatures are higher in this region for both thin and thick plates. Also the peak temperature on the advancing side is slightly higher by 10-15 oK compared to that of the retreating side, it is caused by the tangential velocity vector whose direction is the same as the forward velocity vector on the advance side, but the corresponding direction is contrary to the forward velocity vector on the retreate side.

Figure-10 shows modeling thermal distribution when the tool is moving along welding line at mid position of the workpiece at time 160sec, the temperature distribution effected by heat conduction between the work piece with fixture and by convection, radiation ambient travel speed also has influence on temperature distributions, travel speed and rotating speed on transient temperature distribution. Figures (11), (12) and (13) shows finite element modeling of the distribution of temperature in the transverse direction of welding line in the section B-B when welding tool at mid position of workpiece and according to assumption symmetric value in advance and retreate side Tmax = 642K for (1400rpm-40mm/min), Tmax = 680K for (1400rpm-16mm/min) and Tmax = 605 K for (900rpm-40mm/min).

Figure-14 shows temperature modeled and measured at section B-B when tool position at mid welding line with time 160sec, thermocouples T3, T4 in advance side and T9, T10 in retreate side (the letter T refer to thermocouple number and position), the thermocouples placed at depths 0.5mm below the top surface thermocouple reading shows temperature in advance (T3 = K) is larger than retreate side (T9 = 605.1K).

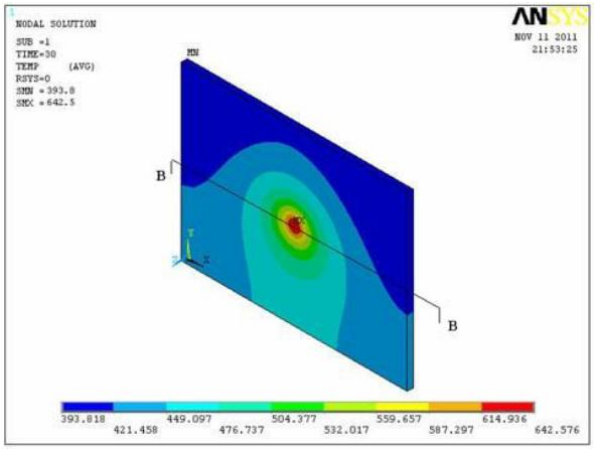

Figure-10. Temperature gradient contour in the top surface of the workpiece at the movement the tool moves to the middle point of the plate (ω = 1400rpm and VT = 40 mm/min).

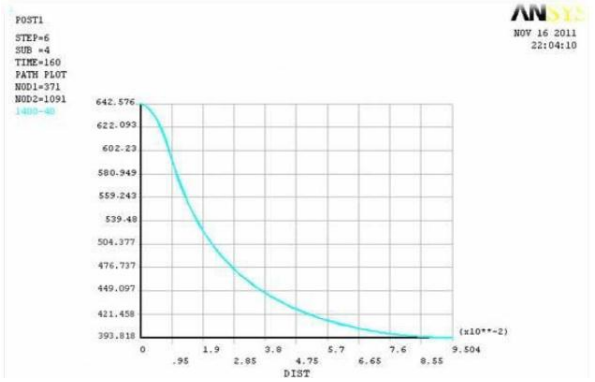

Figure-11. Finite element temperature distribution in mid position in work piece sec B-B in direction perpendicular to welding line at welding parameter (ω = 1400rpm and VT = 40 mm/min).

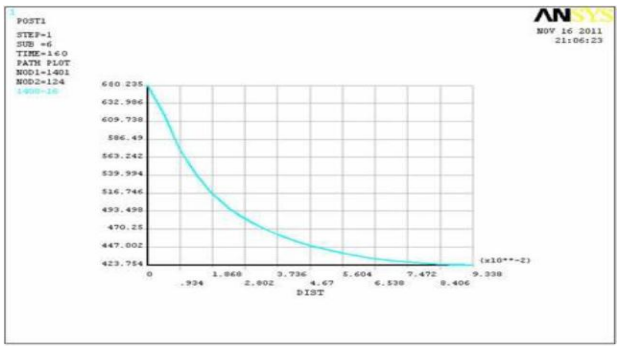

Figure-12. Finite element temperature distribution in mid position in work piece sec B-B in direction perpendicular to welding line at welding parameter (ω = 1400rpm and VT = 16 mm/min).

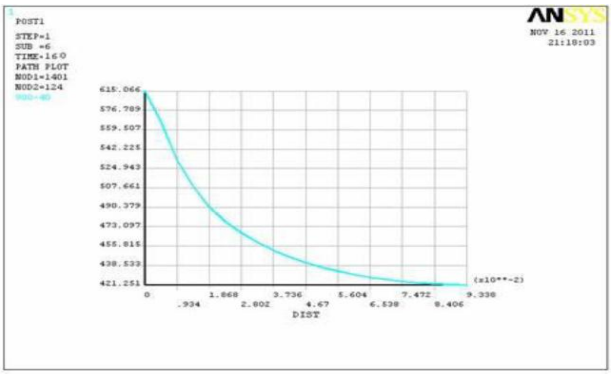

Figure-13. Finite element temperature distribution in mid position in work piece sec B-B in direction perpendicular to welding line at welding parameter (ω = 900rpm and VT =16 mm/min).

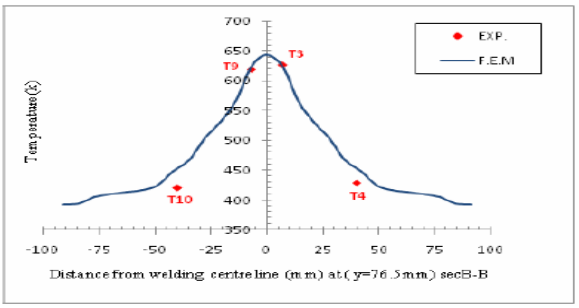

Figure-14. Comparison of F.E.M value and measured temperature distribution along transverse direction welding line at sec. B-B (ω =1400rpm and VT = 40 mm/min).

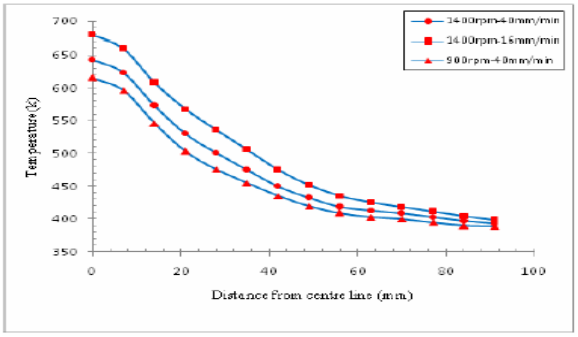

Figure-15. Finite element model values for temperature distribution along transverse direction welding line at sec. B-B at different travel and rotation speeds.

Figure-15 shows finite element modeling temperature distribution along the transverse direction of welding line at y =76.5mm in section B-B at instant when the shoulder's centre passing over this location by travel speeds and rotational speeds (1400rpm, 16mm/min), (1400rpm, 40mm/min) and (900rpm, 40mm/min). It is obvious that the increase of travel speed of the tool will

significantly decrease the temperature of the welded plate; especially in the welding zone and when the rotation speed increase the temperature of workpiece increase because the heat generation input increased [29].

It can be seen that the temperature distribution is more sensitive to changes in the rotational speed compared to the traverse speed, which is in accordance with [30]. Meanwhile, the profiles indicate an asymmetry within the welds with the temperature being higher on the advancing (shear) side than that of the retreating side at different rotary speed. The higher tool traverse speed will induce a lower heat input to the weld zone; the rotary speed determines the quality of heat production and degree of plastic deformation. The traverse speed determines the heat input per unit length of the weld. At higher rotary speed, the peak temperature is higher and forms lots of plastic metal. With the increase of temperature, thermal activation energy provides lots of energy to the dislocation motion and significant residual stress relaxation is likely to occur. Moreover, there is enough time for the stress relaxation due to long cooling times. At lower traverse speed, i.e., higher heat input per unit length, material further away from the weld line is heated up; this results in an increase in the width of the high temperature zone around the tool and a decrease of thermal gradients, thus reducing the thermal expansion mismatch upon cooling, which has been previously observed in the literature [31]

CONCLUSIONS

- Axial load that measured from experimental work decreases with increase in rotational speed because that decrease in strength due to temperature increases in penetration position;
- The experimental data show the maximum temperature measured during FSW at mid position 629k and numerically value from the simulation is 642Ko, which is significantly less than the melting temperature of 7020-T53 aluminum alloy at 916Ko;
- The temperature at advance side (629k) is higher than retreate side (605k);
- Numerical results (Tmax = 642K) agreement with measured data (Tmax = 629k) (error 2%);
- Numerical results show the temperature increases with increase rotating speed (Tmax=642k at1400rpmmm/ min and Tmax=615k at 900rpm-40mm/min); and
- Numerical results show the temperature decrease with increase travel speed (Tmax = 642k at1400rpmmm/ min and Tmax = 680k at 1400rpm-16mm/min).

REFERENCES

[1] Thomas WM, Nicholas ED, Needham JC, Murch MG, Templesmith P and Dawes CJ. 1991. Friction stir welding, international patent application No.PCT/GB92102203 and Great Britain patent application No. 9125978.8.
[2] Salem HG, Reynolds AP and Lyons JS. 2002. Microstructure and retention of super plasticity of friction stir welded super plastic 2095 sheet. Scr. Mater. 46: 337-342.
[3] Nicholas ED and Thomas WM. 1998. A review of friction processes for aerospace applications. Int. J Mater Prod Technol. 13: 45-55.
[4] Tang W, Guo X, McClure J and Murr L. 1998. Heat input and temperature distribution in friction stir welding. J. Mater Process Manuf Sci. 7: 163-172.
[5] Chao Y, Qi X and Tang W. 2003. Heat transfer in friction stirs welding-experimental and numerical studies. Transactions of the ASME. 125: 138-145.
[6] Cao G and Kou S. 2005. Friction stirs welding of 2219 aluminum: behavior of θ (Al2 Cu) particles. Weld J. 84(1): 1s-8s.
[7] Dickerson TL and Przydatek J. 2003. Fatigue of friction stir welds in aluminum alloys that contain root flaws. Int J. Fatigue. 25: 1399-1409.
[8] Guerra M, Schmidt C, McClure JC, Murr LE and Nunes AC. 2003. Flow patterns during friction stir welding. Mater Charact. 49: 95-101.
[9] Li Y, Murr LE and McClure JC. 1999. Solid state flow visualization in the friction stir welding of 2024 Al to 6061 Al. Scr. Mater. 40: 1041-1046.

[10] Colligan K. 1999. Material flow behavior during friction stirs welding of aluminum. Suppl Weld J. 78: 229-237.
[11] Sutton MA, Yang B, Reynolds AP and Taylor R. 2002. Micro structural studies of friction stir welds in 2024-T3 aluminum. Mater Sci Eng A. 323: 160-166
[12] Askari A, Silling S, London B and Mahoney M. 2001. Modeling and analysis of friction stir welding processes. In: Jata KV, Mahoney MW, Mishra RS, Lienert TJ (eds). Friction stir welding and processing. The Minerals Metals and Materials Society, Warren dale. pp. 43-54.
[13] Zhao H. 2005. Friction stir welding (FSW) simulation using an arbitrary Lagrangian-Eulerian (ALE) moving mesh approach, PhD Dissertation, West Virginia University, West Virginia.
[14] Colegrove P, Shercliff H. 2003. 2-Dimensional CFD modeling of flow round profiled FSW tooling. In: Jata KV, Mahoney MW, Mishra RS, Lienert TJ (eds) Friction stir welding and processing. The Minerals Metals and Materials Society, Warren dale. pp. 13-21.
[15] Hyoe T, Colegrove P and Shercliff H. 2003. Thermal and microstructure modeling in thick plate aluminum alloy 7075 friction stir welds. In: Jata KV, Mahoney MW, Mishra RS, Lienert TJ (eds). Friction stir welding and processing. The Minerals Metals and Materials Society, Warren dale. pp. 33-41.
[16] Schmidt H and Hattel J. 2005. A local model for the thermomechanical conditions in friction stirs welding. Model Simul Mater Sci Eng. 13: 77-93.
[17] Nandan R, Roy G and Debroy T. 2006. Numerical simulation of three dimensional heat transfer and plastic flow during friction stir welding. Metall Mater Trans A. 37: 1247-1259.
[18] Ulysse P. 2002. Three-dimensional modeling of the friction stirs welding process. Int. J. Mach Tools Manuf. 42: 1549-1557.
[19] Song M and Kovacevic R. 2003. Thermal modeling of friction stirs welding in a moving coordinate system and its validation. Int. J. Mach Tools Manuf. 43: 605- 615.
[20] Chao Y and Qi X. 1998. Thermal and thermomechanical modeling of friction stir welding of aluminum alloy 6061-T6. J. Mater Process Manuf Sci. 7: 215-233.
[21] Xu SW, Deng XM, Reynolds AP and Seidel TU. 2001. Finite element simulation of material flow in friction stir welding. Sci Technol Weld Joining. 6: 191-193.
[22] 1992. Properties and Selection: Non-Ferrous Alloys and Special Purposes Materials. ASM Handbook, American Society for Metals. Vol. 2.
[23] 2009. ANSYS® Release 12.0 Documentation, ANSYS Inc.
[24] Mohanned Akab. 2006. Investigation of Mechanical and Micro structural Characteristic of Friction Stir Welded Joints. Ph.D. Thesis, University of Baghdad, Iraq.
[25] Sarmad Dhia Ridha. 2010. An investigation of friction stir welding and stress relief by vibration of 6061-T6 aluminum alloy. Ph.D. Thesis. University of Baghdad, Iraq.
[26] Zhu X.K. and Chao Y.J. 2004. Numerical simulation of transient temperature and residual stresses in friction stir welding of 304L stainless steel. Journal of Materials Processing Technology. 146(2): 263-272.
[27] Hansson Sofia. 2006. Simulation of Stainless Steel Tube Extrusion. Luleå University of Technology, Sweden.
[28] Dixon John, Burkes Douglas and Medvedev Pavel 2007. Thermal Modeling of a Friction Bonding Process. Proceedings of the COMSOL Conference, Boston.
[29] Chen C.M. and Kovacevic R. 2003. Finite element modeling of friction stir welding - thermal and thermomechanical analysis. International Journal of Machine Tools and Manufacture. 43(13): 1319-1326.
[30] Steuwer A, Peel MJ and Withers PJ. 2006. Dissimilar friction stir welds in AA5083- AA6082: the effect of process parameters on residual stress. Mater Sci Eng A. 441(1-2): 187-196.
[31] Lombard H, Hattingh DG, Steuwer A and James MN. 2009. Effect of process parameters on the residual stresses in AA5083-H321 friction stir welds. Mater Sci Eng A. 501(1-2): 119-124.